1 UPMC Univ Paris 06, UMR_S938 CDR Saint-Antoine, Prolifération et Différentiation des Cellules Souches, F-75012 Paris, France

2 INSERM, UMR_S938, Prolifération et Différentiation des Cellules Souches, F-75012 Paris, France

3 AP-HP, Hôpital St Antoine et Hôpital Trousseau, Service d'Hématologie et Immunologie Biologiques, F- 75012 Paris, France

4 EFS Ile de France, Unité d'Ingénierie et de Thérapie Cellulaire, Créteil, F-94017, France

5 Laboratory of Excellence GR-Ex, Paris, France

6 Institut National de Transfusion Sanguine INTS, F- 75012 Paris, France

7 IFR 65-Saint Antoine UMPC, Plateforme de Cy-tométrie, F-75012 Paris, France

8 CNRS UMR7622, Laboratoire de biologie et du développement, F-75005 Paris, France

9 UPMC UMR7622, Laboratoire de biologie et du développement, F-75005 Paris, France

Molecular Signature of Erythroblast Enucleation in Human Embryonic Stem Cells

SHAGHAYEGH ROUZBEH[1,2,5], LADAN KOBARI[1,2,5], MARIE CAMBOT[6], CHRISTELLE MAZURIER[1,2,4,5], NICOLAS HEBERT[1,2,4,5], ANNE-MARIE FAUSSAT[7], CHARLES DURAND[8,9], LUC DOUAY[1,2,3,4,5] AND HÉLÈNE LAPILLONNE[1,2,3,5]

Key words. Embryonic stem cells • Erythropoiesis • Enucleation • miR-30a

ABSTRACT

While enucleation is a critical step in the terminal differentiation of human red blood cells, the molecular mechanisms underlying this unique process remain unclear. To investigate erythroblast enucleation we studied the erythroid differentiation of human embryonic stem cells (hESCs), which provide a unique model for deeper understanding of the development and differentiation of multiple cell types. Firstly, using a two-step protocol, we demonstrated that terminal erythroid differentiation from hESCs is directly dependent on the age of the embryoid bodies. Secondly, by choosing hESCs in two extreme conditions of erythroid culture, we obtained an original differentiation model which allows one to study the mechanisms underlying the enucleation of erythroid cells by analyzing the gene and miRNA (miR) expression profiles of cells from these two culture conditions. Thirdly, using an integrated analysis of mRNA and miR expression profiles, we identified 5 miRs potentially involved in erythroblast enucleation. Finally, by selective knockdown of these 5 miRs we found miR-30a to be a regulator of erythroblast enucleation in hESCs. STEM CELLS *2015; 00:000–000*

INTRODUCTION

Erythropoiesis is a multi-stage process during which a hematopoietic stem cell undergoes a series of differentiation steps to generate mature and enucleated erythrocytes. As erythroblasts mature, they decrease in size, synthesize more hemoglobin and undergo membrane reorganization and chromatin condensation, which terminates in extrusion of the nucleus before the cells take up a biconcave discoid structure [1, 2]. While enucleation is the final step in the development of mature erythrocytes, the molecular mechanisms involved in this process are poorly understood.

Identifying the specific genes expressed during erythropoiesis will be essential to understand erythroid developmental biology and to elucidate the mechanisms involved in the terminal differentiation of red blood cells, which in turn will help us to optimize the conditions for efficient generation of cultured red blood cells (cRBC).

The mechanisms reported to play a central role in terminal erythroid differentiation and enucleation may be classified in two main groups: (1) nuclear modifications including chromatin condensation and processes involving transcriptional factors and miRs and (2) cellular processes including protein sorting, membrane maturation, vesicle trafficking and cytoskeletal remodeling [3-8].

Recent studies have shown that miRs play an important role in the proliferation, differentiation and terminal differentiation of erythroid cells [9-15]. In late erythropoiesis, miR-144/451 and miR-191 were identified as regulators of erythroid differentiation [16-18], while miR-451 plays a role in mediating erythropoiesis by repressing negative regulators of erythroid differentiation such as *GATA2* [19]. In 2011, Zhang et al showed that erythroid enucleation in mice requires the down-regulation of miR-191 through the derepression of *RIOK3* and *MXI1* translation, consistent with the essential role of these genes in chromatin condensation [18].

Our team has described all the major steps towards the generation of cRBCs for transfusion purposes: *in vitro* production of cRBCs from CD34+ hematopoietic cord blood stem/progenitor cells [20], *in vitro* generation of cRBCs from pluripotent stem cells [21], the first injection of cRBCs into human donors [22] and recently complete terminal erythroid maturation of human induced pluripotent stem cells *in vivo* [23]. Pluripotent stem cells appear to be the best cell source for our purposes. They also provide a unique model for fundamental research, to investigate the different stages of erythropoiesis, especially terminal maturation and in particular the mechanisms involved in the enucleation of erythroblasts. Enucleation remains one of the critical steps of *in vitro* RBC production, especially starting from pluripotent stem cells.

In this work, using a model of erythroid differentiation in hESCs, we found that terminal erythroid differentiation is directly dependent on the age of the embryoid bodies (EBs) and determined the expression profiles of mRNAs and miRs in erythroid cells derived from early and late EBs. Subsequent integrated analysis of mRNA and miR expression profiles during terminal erythroid differentiation allowed us to identify several genes and miRs potentially involved in erythroblast enucleation. Finally, knockdown studies of candidate miRs led us to identify miR-30a as a key regulator of erythroblast enucleation in hESCs.

MATERIALS AND METHODS

Cells and culture conditions

The research on embryonic stem cells was authorized by the French Biomedicine Agency (R0500225A, R0500226A and R0500227A). The hESC lines H1 and H9 (National Institute of Health [NIH]: code WA01, passages 28-30 and code WA09, passages 27-33) were maintained in an undifferentiated state by weekly mechanical passage on Matrigel (BD Biosciences, San Jose, CA, USA). Matrigel was diluted in KO-DMEM (1:100) and used to coat tissue culture dishes for 1 h at room temperature. After coating, the Matrigel solution was completely removed and mTeSR-1 medium (Stemcell Technologies, Vancouver, Canada) was added to the coated dishes. Thereafter the medium was changed on a daily basis. The normal karyotype of H1-hESCs and H9-hESCs was confirmed by performing karyotyping analysis at passage 24 and passage 26 respectively.

For erythroid induction and differentiation we used a two-step protocol adapted from our previous procedures [20, 21, 23]. To allow hEB formation, undifferentiated hESCs were treated with collagenase IV (1 mg/mL; Invitrogen) and transferred to low attachment plates (Nunc) in liquid culture medium (LCM: IMDM [Biochrom], 450 µg/mL holo-human transferrin [Scipac], 10 µg/mL recombinant human insulin [Incelligent SG, CellGen], 2 IU/mL heparin and 5% human plasma) in the presence of stem cell factor (SCF, 100 ng/mL), thrombopoietin (TPO, 100 ng/mL), FLT3 ligand (FL, 100 ng/mL), recombinant human bone morphogenetic protein 4 (BMP4, 10 ng/mL), recombinant human vascular endothelial growth factor (VEGF-A165, 5 ng/mL), interleukin-3 (IL-3, 5 ng/mL), interleukin-6 (IL-6, 5 ng/mL) (Peprotech) and erythropoietin (Epo, 3 U/mL) (Eprex, kindly provided by Janssen-Cilag, France). hEBs were cultured for 9 days or 20 days at 37°C in a humidified 5% CO_2 atmosphere. The cells were then dissociated into a single cell suspension by incubation with collagenase B (0.4 U/mL; Roche Diagnostics, Laval, QC, Canada) for 30 min at 37°C followed by cell dissociation buffer (Invitrogen) for 10 min at 37°C.

The erythroid protocol (days 0 to 31) was adapted from our previous procedures for EB9 and EB20 [21, 23]. On day 0 dissociated hEBs were plated at a density of $1x10^6$ cells/mL in LCM containing 10% human plasma,

heparin (3 U/mL), SCF (100 ng/mL), IL-3 (5 ng/mL) and Epo (3 U/mL). On day 8 the cells were resuspended at a density of $3x10^5$ to $1x10^6$ cells/mL and cultured in fresh medium supplemented with SCF (100 ng/mL) and Epo (3 U/mL). On day 18 the cells were resuspended at a density of $2x10^6$ or $5x10^6$ cells/mL and cultured until day 31 in fresh medium supplemented with Epo (3 U/mL). The cultures were maintained at 37°C in 5% CO_2 in air. To evaluate the maturation and enucleation of erythroblast, from day 4 to 25, $1\text{-}2x10^5$ cells were washed and spun onto slides by cytocentrifugation. Cytological examinations were performed on slides stained with May-Grunwald Giemsa (Sigma). The percentage of enucleation was determined by counting at least 500 cells per slide.

FACS analysis and sorting

Samples were analyzed using a FACSCalibur flow cytometer with CellQuest acquisition software (Becton Dickinson, San José, CA, USA). The following antibodies were used for flow cytometric analysis: SSEA4-PE (phycoerythrin) and SSEA1-PE (Clinisciences, Montrouge, France); TRA-1-60, TRA-1-81, goat anti-mouse IgM-PE and goat anti-mouse IgG-PE (Chemicon, Saint-Quentin en Yvelines, France); CD34-PE, CD45-PE, CD45-PC7, CD71-FITC, CD36-FITC and CD235a-PE (glycophorin A) (Beckman Coulter, Immunotech, Marseille, France). Hoechst 33342 was used for nuclei detection (Invitrogen). For miRNA knock-down experiments, green fluorescent protein (GFP)-positive *in vitro* cultured erythroid cells were sorted on a MoFloAstrios Cell Sorter (Beckman Coulter), 96 h after transduction.

Total RNA isolation

Total human RNA was isolated with Trizol (Sigma-Aldrich). RNA quality and integrity were determined using an Agilent RNA 6000 Nano Kit and an Agilent 2100 Bioanalyzer (Agilent Technologies). RNA was quantified by measuring the absorption at 260 nm on an ND-1000 Spectrophotometer (NanoDrop Technologies).

Microarray design and analysis

Microarray analysis was performed in triplicate and the samples were selected on the basis of the RNA integrity (RIN>8.1). A total of 12 RNA samples were hybridized with 12 Agilent 4X44K Whole Human Genome Oligo microarrays (One-color) and with 12 miRXplore™ microarrays. Detailed information of microarray experimental procedures is provided in the supplemental data. The data discussed in this manuscript were submitted to the NCBI Gene Expression Omnibus and are accessible through the GEO Series accession number GSE55532
(http://www.ncbi.nlm.nih.gov/geo/query/acc.cgi?token = uvslgkccxxgrjir&acc=GSE55532).

Quantitative PCR analysis

RNA (1 µg) taken from individual samples was treated with DNAse and cDNA was synthesized using a High Capacity cDNA Reverse Transcription Kit (Applied Biosystems, Foster City, CA, USA). Quantitative polymerase chain reaction (qPCR) analysis was performed using a TaqMan® Universal PCR Fast Master Mix (Applied Biosystems) with Taqman® primers and probes from Applied Biosystems. The expression data for each transcript were normalized to those for the reference gene GAPDH and for expression of the same gene in Universal cDNA (Clontech).

For miRNA expression, RNA from cells derived from H1 and H9 hESCs was reverse transcribed using a TaqMan® MicroRNA reverse transcription kit and TaqMan® MicroRNA assays (Applied Biosystems) specific for the mature form of miRs, with human RNU6B and RNU48 for normalization to an endogenous control. Real-time PCR amplification was carried out using standard TaqMan® PCR reagents and TaqMan® MicroRNA assays for the differentially expressed miRs, with human *U6* and *U48* controls (all from Applied Biosystems). Triplicate analyses were run for each sample and data were collected with 7500 System Sequence Detection Software (Applied Biosystems). One tail student's t-test was carried out to determine the statistic significances.

Knockdown of miRNAs

Pseudoviral particles for miRNA knockdown were generated using lentivector-based anti-miRNA constructs as instructed by the manufacturer (miRZIP, System Biosciences, Mountain View, CA, USA). EB9-derived erythroid cells were transduced with pseudoviral particles (MOI 10) containing vectors coding for anti-miRNAs on day 4 of culture. Stably expressing cells were selected on day 8 of culture by green fluorescent protein-based cell sorting.

RESULTS

We have previously developed robust culture conditions for the *ex vivo* generation of cRBCs from both fetal and adult human induced pluripotent stem cells (hiPSCs) and hESCs [21]. In this study, our protocol comprised two steps: (1) differentiation of hESCs through formation of hEBs in the presence of cytokines and human plasma to induce mesodermic and early erythroid commitment and (2) differentiation/maturation to form cRBCs in the presence of cytokines without co-culture on a cellular stroma.

Erythroid differentiation and maturation

Differentiation of hESCs into hEBs conditioned for erythroid commitment

Using our protocol we intended to identify the stage of differentiation of hEBs having the best erythroid potential. We therefore studied early hEBs from day 9 (called

EB9-D0) and late hEBs from day 20 (called EB20-D0) by following the expression of specific markers of hematopoiesis and erythropoiesis by flow cytometry. Prior to their differentiation, hESCs expressed high levels of a marker of undifferentiated human cells (SSEA4). As expected the expression of SSEA1 (stage-specific embryonic antigen 1) was low and hematopoietic markers (CD45, CD34, CD36 and CD235a) were undetectable. During hEB differentiation, expression of the marker of undifferentiated human cells decreased significantly and remained weakly positive. EB9-D0 and EB20-D0 expressed hematopoietic and erythroid markers such as CD45, CD34, CD45/CD34, CD71 and CD235a. EB20-D0 cultures displayed more cells expressing CD45, CD235a and CD36 than EB9-D0 cultures (Table 1A).

Differentiation/maturation of hEBs into erythroid cells

Dissociated hEBs from both EB9-D0 and EB20-D0 cultures were replated using our liquid culture protocol for erythroblastic differentiation/maturation as previously described [21, 23]. Erythroid maturation was evaluated regularly according to the cell morphology after staining with May-Grünwald-Giemsa (MGG) and the expression of erythroid membrane antigens as determined by flow cytometry.

The erythroid commitment of hEBs was complete after 8 days of liquid culture with up to 95% production of erythroblasts from both EB9 and EB20 populations. On day 25 the EB20 population contained 42 to 65% enucleated cRBCs and 38 to 45% orthochromatic erythroblasts. In contrast, on day 25 we observed no enucleated cells in EB9 cultures and all the cells were blocked at the orthochromatic megaloblastic stage (Figure 1A and Table 1B). At the end of erythroid culture, on day 31 almost no enucleated cells had been generated from EB9 cells.

Flow cytometric analysis of the cells confirmed their degree of maturity. In both populations, by day 18 the cultured erythroid cells strongly expressed CD235a and CD71 (Figure 1B). Depending on the duration of EB culture, we obtained either a substantial percentage of enucleated cRBCs (up to 65%: 55±11 for EB20-D25) or no enucleation (less than 1%: 0.6±0.5 for EB9-D250).

Transcriptome analysis during erythroid differentiation

To identify the molecular mechanisms involved in terminal erythroid differentiation, we compared the gene and miRNA expression profiles of the erythroid populations obtained from early hEBs (EB9) and late hEBs (EB20) on day 18 (EB9-D18 versus EB20-D18) of erythroid culture starting from hESCs H1. On day 18 each condition displays the most morphologically and phenotypically homogeneous cell populations representing late erythroblast populations containing mostly orthochromatophilic erythroblast/reticulocytes (Figure 1, Table 1B).

Due to the large number of differentially expressed genes, we performed several levels of analysis in order to define more specific gene categories which were repressed or strongly present in EB9 as compared to EB20 cells. Supplemental Figure 1 presents an overview of the experiments.

Level I of analysis: Genes differentially expressed in EB9-D18 versus EB20-D18 cultures

Pairwise comparisons of gene expression between EB9-D18 and EB20-D18 samples were considered to be significant if the *P* value was ≤ 0.05 and the fold change ≥ 2 (log2 = 1).

A total of 3638 reporters fulfilled our selection criteria after comparison of cultured cells blocked in terminal erythroid differentiation (EB9-D18) with cells, which had fully differentiated (EB20-D18). This corresponded to 1278 up-regulated reporters and 2360 down-regulated reporters in EB9-D18 as compared to EB20-D18 cultures (Supplemental Table 1). Among the down-regulated genes in EB9-D18 samples, we found erythroid-specific genes of several classes including transcription factors and regulators such as *SOX6*, *MYB*, *FOXO3*, *E2F2* and *ID2*, genes playing a key role in erythroid maturation and enucleation like *RIOK3*, *MXI1*, *RAC2* and *BNIP3L*, signaling molecules like *MAP2K3* and *PIK3* and genes associated with apoptosis such as *BIRC3*, *HMOX1* and *BCL6*. The complete list of differentially expressed (DE) reporters with intensities for each sample is given in Supplemental Table 1.

Validation of gene expression by quantitative PCR analysis

RT-qPCR analysis confirmed the array signal intensity for a selection of differentially expressed genes with expression ratios greater than those observed using the microarray (Figure 2A).

miRs differentially expressed in EB9-D18 as compared to EB20-D18 cells

DE miRs were required to have a corrected *P* value of less than or equal to 0.05 and at least a 2-fold change in expression level.

We identified 35 miRs with at least a 2-fold higher mean expression in EB9-D18 cells, while 26 miRs displayed lower expression in EB9-D18 as compared to EB20-D18 cells (Supplemental Table 2). As a result, the majority of miRs were more strongly expressed in EB9-D18 cultures. This was to be expected since these cells were blocked in terminal differentiation and should thus represent a less differentiated cell type. It also correlates with the whole genome analysis as we found a greater number of genes to be repressed in EB9-D18 as compared to EB20-D18 cultures.

Gene set enrichment (GSE) analysis

GSE analysis of the genes more strongly expressed in EB9-D18 cultures revealed only a few categories. These

gene sets were however enriched for cell differentiation and regulation of cellular processes and cell development (Table 2A). Genes more weakly expressed in EB9-D18 cultures were enriched in categories associated with the immune response, predominantly related to regulation of this response and cell surface receptor-linked signaling pathways (Table 2B).

Level II of analysis: Comparison of EB20-D18 versus EB20-D0 and EB9-D18 cells

To identify a gene signature involved in the final step of erythroid differentiation, we compared the list of up-regulated genes in EB20-D18 cells with those in EB20-DO and EB9-D18 cells. We found 1397 commonly up-regulated genes in the two settings (Figure 2B, Supplemental Table 3). Interestingly, GSE analysis of the overlapping genes revealed several categories mostly present in erythroid cells, with strongest enrichment of the *FOXO* family implicated in signaling and protein degradation pathways (Figure 2C). Genes belonging to these most significantly enriched categories included the transcription factor *FOXO3* and its transcriptional targets involved in erythropoiesis such as the cyclin-dependent kinase inhibitor *CDKN1B*, *CREBBP* which is a co-activator in erythroid differentiation and anti-oxidant gene catalysis (*CAT*) and sets of genes associated with autophagy and the formation of autophagic vacuoles like *ULK1*, *PI3K*, *GABARAPL1/2* and *MAP1LC3A/B.*

Level III of analysis: Integrated analysis of miRNA and mRNA transcriptomes

In an effort to perform a robust integrative analysis, we combined the mRNA and miRNA expression profiles on day 18 of erythroid culture and then carried out GSE analysis to identify associated pathways and biological functions which are altered during the terminal phase of erythroid differentiation.

Lists of potential and validated targets of over-expressed miRs were established using eight target prediction algorithms: miRDb [41], PicTar [42], DIANAmT [43], miRanda [44], PITA [45], RNAhybrid and TargetScan [46] and miRWalk [24]. In order to combine the mRNA and miR expression data, we compared potential and validated targets for 35 up-regulated miRs of EB9-D18 cells with genes down-regulated in EB9-D18 as compared to EB20-D18 cells. A total of 1026 repressed genes were found to be potential targets of miRs and 127 repressed genes to be validated targets (Supplemental Table 4-5).

Combining the 35 up-regulated miRs and the 1026/127 down-regulated genes, we found 5 miRs to be the most frequently appearing candidates: miR-34a, miR-9, miR-30a, miR-221 and Let-7e.

miR-30a modulates erythroblast enucleation

To determine whether down-regulation of miR-34a, miR-9, miR-30a, miR-221 or Let-7e correlates with erythroid enucleation, we transduced day 4 erythroid cells from EB9 cultures with a lentivirus harboring anti-miR (miRZIP). On day 8 of erythroid culture, GFP-positive transduced cells were sorted and cultured until day 25.

On day 25, the enucleation status of anti-miR-infected cells was determined by MGG staining, as compared to controls. Knockdown of Let-7e or miR-221 had no effect on terminal erythroid enucleation (data not shown). Knockdown of miR-34a or miR-9 slightly increased enucleation with 13-15% enucleated cells. Strikingly, knockdown of miR-30a significantly increased the enucleation of erythroblasts with 51±10% enucleated cells as compared to cells infected with a scramble vector, which generated 0.4±0.3% enucleated cells (Figure 3A, Supplemental Figure 2). Importantly we didn't observe any significant difference in the rate of proliferation of erythroid cells in miRZIP-30a infected EB9 cells compared to controls (Table 1C).

RT-qPCR analysis of the expression of miR-9, miR-34a and miR-30a showed that the level of miR expression in anti-miR cells was significantly inhibited relative to that in cells infected with a scramble vector control (Figure 3B).

The up-regulation of these 3 miRs was also detected in erythroid cells derived from hESC H9-EB9 as compared to H9-EB20 cells, and was correlated with the absence of enucleation in H9-EB9 cells (Figure 4A). The inhibitory effect of miR-30a on the enucleation of erythroblasts was confirmed in H9-EB9-derived erythroid cells using the same approach (Supplemental Figure 3)

The miR-30a expression pattern during culture of erythroblasts derived from H1 and H9 cells is shown in Figure 4B for early and late EBs. To further explore the correlation between expression of miR-30a and enucleation of erythroblasts, we analyzed the expression kinetics of miR-30a during erythroid differentiation of CD34+ cells from human cord blood. As shown in Figure 4C, the expression of miR-30a decreased significantly during erythroid differentiation, concomitant with an increase in the rate of enucleation of erythroblasts derived from CD34+ cells (Figure 4C-D). Flow cytometric analysis of miRZIP-30a infected EB9 cells did not show any significant difference in expression of erythroid markers as compared to control (Supplemental Figure 4).

Correlation between miR-30a and gene expression

RT-qPCR analysis was employed to search for putative target genes affected by miR-30a inhibition in anti-miR-30a (miRZIP-30a)-transduced cells. Candidate genes were selected among putative miR-30a target genes down-regulated in EB9-D18 as compared to EB20-D18 cells in the mRNA transcriptome results. The expression profiles of miRZIP-30a-transduced cells were compared to those of control cells, i.e., EB9 control cells and cells infected with a scramble vector. Among 30 genes analyzed, we found that knockdown of miR-30a significant-

ly increased the expression of several potential target genes including *RIOK3*, *HDAC5*, *BNIP3L*, *GABARAPL1/2* and *MAP1LC3B* (Figure 5).

DISCUSSION

We investigated the expression profiles of genes and miRs during erythroid differentiation in a hESC EB system and showed that the terminal erythroid differentiation capacity of hESCs is directly depended on the age of the EBs. Only late EBs reached the final step of erythroid maturation, i.e., enucleation. In 2007, Dong Chen et al analyzed the definitive hematopoiesis commitment of hemangioblasts in hESC-derived EBs. These authors determined the gene expression in EBs by microarray analysis at five specific time points and observed that the transition from primitive to definitive hematopoiesis occurs on day 12 [25]. We then performed a microarray analysis of EB9 and EB20 cells as representing two extreme time points in erythroid differentiation, in order to explore the molecular mechanisms underlying embryonic terminal erythroid differentiation. By performing two types of microarray experiment, we identified several categories of genes and miRs differentially expressed in cells blocked in the course of terminal erythroid differentiation as compared to those undergoing enucleation.

Applying different levels of analysis to day 18 cell samples and combining the miR and mRNA expression data, we identified five miRs potentially involved in the enucleation hESCs: miR-34a, miR-9, miR-30a, miR-221 and Let-7e. Furthermore, by targeting these 5 miRs in knockdown experiments we demonstrated an inhibitory effect of miR-30a on erythroblast enucleation. Knockdown of miR-30a resulted in a major increase in enucleated cells in EB9 cultures, with a rate of enucleation comparable to that observed in EB20 cultures.

miR-30a is identified as a negative regulator of autophagy by targeting some autophagy-related genes in myocardial hypertrophy and cancer cells [26-28]. Although the role of miR-30a in erythropoiesis is less understood, some studies have reported its increased expression during murine erythroid differentiation and the erythropoiesis of CD34+ cells derived from human cord blood [29, 30]. In our study, we observed an increase in miR-30a expression during the differentiation of H1/H9 hESC-derived erythroblasts, which undergo erythroid differentiation but fail to extrude their nuclei, unlike those which give rise to mature enucleated cells. Interestingly, hiPSC-derived erythroblasts display a low rate of enucleation and express high levels of miR-30a (data not shown).

To further explore the molecular mechanisms of the functions of miR-30a, we performed RT-qPCR assays to identify candidate genes involved in the miR regulation network. A first series of results revealed a significant increase in the expression of several candidate targets which might be directly regulated by miR-30a. The genes affected by miR-30a inhibition included *RIOK3*, *HDAC5*, *BNIP3L*, *GABARAPL1*, *GABARAPL2* and *MAP1LC3B*.

Riok3 belongs to the RIO family of atypical protein kinases and it was recently shown by Zhang et al that knockdown of Riok3 blocks chromatin condensation and the enucleation of erythroblasts in mouse fetal liver cells [18]. Several studies have investigated the role of chromatin condensation in erythroblast enucleation [1, 2, 18]. In 2009, Popova et al reported that *HDAC5* was significantly up-regulated during the terminal stages of differentiation of Friend virus-infected erythroblasts. Moreover, treatment with trichostatin A, a histone deacetylase inhibitor, blocked both chromatin condensation and nuclear extrusion. Contrary to these results, Peng et al found *HDAC2* but no other *HDAC* to be an important regulator in mediating chromatin condensation and enucleation during the final stages of mammalian erythropoiesis [1]. In our study *HDAC4*, *HDAC6*, *HDAC8* and *HDAC9* were significantly expressed in both EB9- and EB20-derived cells during the late stages of erythropoiesis, whereas *HDAC5* was only expressed in EB20-derived erythroid cells, which underwent enucleation. Our microarray results showed no difference in the expression of *HDAC2* between EB9 and EB20-derived cells on day 18. Nevertheless, much remains to be learned about the mechanisms and proteins employed by erythroid cells to condense their nucleus.

The ATG8 family members in humans, *GABARAPL1*, *GABARAPL2*, *MAP1LC3A* and *MAP1LC3B,* associate with autophagic vesicles and their up-regulation strongly induces autophagy [31-35]. The fact that ATG8 proteins interact with numerous RAB GTPase regulatory proteins also points to a role of ATG8 in controlling localized RAB activation and vesicle dynamics [36].

Several lines of evidence support the hypothesis that formation of cytoplasmic vesicles and autophagic vacuoles contributes to enucleation [4, 5]. Recently, Keerthivasan et al showed that vesicle trafficking, in particular the formation and movement of vacuoles at the junction of the nucleus and the cytoplasm, is a critical component of mammalian erythroblast enucleation [4, 5]. There is likewise evidence supporting a link between autophagy and vesicle trafficking [37]. Autophagy is an important phenomenon which takes place during enucleation and involves the segregation of cellular components such as organelles and proteins [3, 38] Several studies have demonstrated the role of *BNIP3L* (*Nix*), a member of the Bcl-2 family, in mitochondrial clearance during reticulocyte maturation. Sandoval et al reported that Nix-/- mice developed anemia with reduced mature erythrocytes, although in this study loss of Nix did not affect enucleation [7]. It has been reported that *BNIP3L* interacts with *GABARAPL1* and *MAP1LC3A*, pointing to a direct link with the autophagosome biogenesis pathway [38, 39].

A recent study of erythroid differentiation showed that autophagy is induced at the polychromatic erythroid stage and that autophagosomes remain abundant until enucleation. These authors observed

that this stimulation was associated with the transcriptional up-regulation of many autophagy genes including all members of the ATG8 mammalian paralog family [40]. However, there is to date no study investigating the direct role of autophagy and autophagy-associated genes such as *GABARAPL1*, *GABARAPL2* and *MAP1LC3B* in the enucleation process and further experiments will be needed to explain the link between autophagy and the terminal differentiation of erythroblasts.

In conclusion, we present a unique *in vitro* model of erythropoiesis in hESCs to explore gene and miRNA expression changes during terminal erythroid differentiation. On the basis of our observations we could identify miR-30a as a regulator of erythroblast enucleation. We also investigated the expression of putative target genes affected by miR-30a inhibition. Further functional studies will be required to confirm the direct interaction of these putative target genes with miR-30a and their roles in the enucleation of hESCs. Our observation is nevertheless a major step towards improving the enucleation of erythroblasts and opens a new field for the *in vitro* production of RBCs from pluripotent stem cells.

ACKNOWLEDGMENTS

This work was supported by a Labex GR-Ex fellowship. The Labex GR-Ex, reference ANR-11-LABX-0051, is funded by the program "Investissements d'avenir" of the French National Research Agency, reference ANR-11-IDEX-0005-02, the Etablissement Français du Sang (EFS), the association "Fondation pour la recherche médicale", the association "Combattre La Leucémie" and the DIM Stempôle (Paris, France). We would also like to thank Thierry Jaffredo and Olivier Hermine for helpful discussions.

CONFLICT-OF-INTEREST DISCLOSURE

The authors declare that they have no conflict of interest.

AUTHOR CONTRIBUTIONS

S.R.: Conception and design, Data analysis and interpretation, Manuscript writing; L.K.: Design of cell culture; M.C.: Lentiviruses production; C.M.: Flow cytometry experiments; N.H.: Technical assistance for cell culture and PCR analyses; A.-M.F.: Cell sorting; C.D.: Assistance for microarray interpretation; L.D.: Supervision of the overall research; H.L.: Conception and design, Supervision of the overall research, Manuscript writing

REFERENCES

1 Ji P, Yeh V, Ramirez T et al. Histone deacetylase 2 is required for chromatin condensation and subsequent enucleation of cultured mouse fetal erythroblasts. **Haematologica**. 2010;95:2013-2021.

2 Popova EY, Krauss SW, Short SA et al. Chromatin condensation in terminally differentiating mouse erythroblasts does not involve special architectural proteins but depends on histone deacetylation. **Chromosome Res**. 2009;17:47-64.

3 Chen M, Sandoval H, Wang J. Selective mitochondrial autophagy during erythroid maturation. **Autophagy**. 2008;4:926-928.

4 Keerthivasan G, Liu H, Gump JM et al. A novel role for survivin in erythroblast enucleation. **Haematologica**. 2012;97:1471-1479.

5 Keerthivasan G, Small S, Liu H et al. Vesicle trafficking plays a novel role in erythroblast enucleation. **Blood**. 2010;116:3331-3340.

6 Sandoval H, Thiagarajan P, Dasgupta SK et al. Essential role for Nix in autophagic maturation of erythroid cells. **Nature**. 2008;454:232-235.

7 Zhang J, Ney PA. Role of BNIP3 and NIX in cell death, autophagy, and mitophagy. **Cell Death Differ**. 2009;16:939-946.

8 Watanabe S, De Zan T, Ishizaki T et al. Loss of a Rho-regulated actin nucleator, mDia2, impairs cytokinesis during mouse fetal erythropoiesis. **Cell Rep**. 2013;5:926-932.

9 Bianchi N, Zuccato C, Finotti A et al. Involvement of miRNA in erythroid differentiation. **Epigenomics**. 2012;4:51-65.

1**0** Listowski MA, Heger E, Boguslawska DM et al. microRNAs: fine tuning of erythropoiesis. **Cell Mol Biol Lett**. 2013;18:34-46.

1**1** Felli N, Fontana L, Pelosi E et al. MicroRNAs 221 and 222 inhibit normal erythropoiesis and erythroleukemic cell growth via kit receptor down-modulation. **Proc Natl Acad Sci U S A**. 2005;102:18081-18086.

1**2** Felli N, Pedini F, Romania P et al. MicroRNA 223-dependent expression of LMO2 regulates normal erythropoiesis. **Haematologica**. 2009;94:479-486.

1**3** Gabbianelli M, Testa U, Morsilli O et al. Mechanism of human Hb switching: a possible role of the kit receptor/miR 221-222 complex. **Haematologica**. 2010;95:1253-1260.

1**4** Sankaran VG, Menne TF, Scepanovic D et al. MicroRNA-15a and -16-1 act via MYB to elevate fetal hemoglobin expression in human trisomy 13. **Proc Natl Acad Sci U S A**. 2011;108:1519-1524.

1**5** Wang Q, Huang Z, Xue H et al. MicroRNA miR-24 inhibits erythropoiesis by targeting activin type I receptor ALK4. **Blood**. 2008;111:588-595.

1**6** Bruchova-Votavova H, Yoon D, Prchal JT. miR-451 enhances erythroid differentiation in K562 cells. **Leuk Lymphoma**. 2010;51:686-693.

1**7** Masaki S, Ohtsuka R, Abe Y et al. Expression patterns of microRNAs 155 and 451 during normal human erythropoiesis. **Biochem Biophys Res Commun**. 2007;364:509-514.

1**8** Zhang L, Flygare J, Wong P et al. miR-191 regulates mouse erythroblast enucleation by down-regulating Riok3 and Mxi1. **Genes Dev**. 2011;25:119-124.

1**9** Pase L, Layton JE, Kloosterman WP et al. miR-451 regulates zebrafish erythroid maturation in vivo via its target gata2. **Blood**. 2009;113:1794-1804.

2**0** Giarratana MC, Kobari L, Lapillonne H et al. Ex vivo generation of fully mature human red blood cells from hematopoietic stem cells. **Nat Biotechnol**. 2005;23:69-74.

2**1** Lapillonne H, Kobari L, Mazurier C et al. Red blood cell generation from human induced pluripotent stem cells: perspectives for transfusion medicine. **Haematologica**. 2010;95:1651-1659.

2**2** Giarratana MC, Rouard H, Dumont A et al. Proof of principle for transfusion of in vitro-generated red blood cells. **Blood**. 2011;118:5071-5079.

2**3** Kobari L, Yates F, Oudrhiri N et al. Human induced pluripotent stem cells can reach complete terminal maturation: in vivo and in vitro evidence in the erythropoietic differentiation model. **Haematologica**. 2012;97:1795-1803.

2**4** Dweep H, Sticht C, Pandey P et al. miRWalk--database: prediction of possible miRNA binding sites by "walking" the genes of three genomes. **J Biomed Inform**. 2011;44:839-847.

2**5** Chen D, Wang P, Lewis RL et al. A microarray analysis of the emergence of embryonic definitive hematopoiesis. **Exp Hematol**. 2007;35:1344-1357.

2**6** Zhu H, Wu H, Liu X et al. Regulation of autophagy by a beclin 1-targeted microRNA, miR-30a, in cancer cells. **Autophagy**. 2009;5:816-823.

2**7** Yu Y, Yang L, Zhao M et al. Targeting microRNA-30a-mediated autophagy enhances imatinib activity against human chronic myeloid leukemia cells. **Leukemia**. 2012;26:1752-1760.

2**8** Pan W, Zhong Y, Cheng C et al. MiR-30-regulated autophagy mediates angiotensin II-induced myocardial hypertrophy. **PLoS One**. 2013;8:e53950.

2**9** Choong ML, Yang HH, McNiece I. MicroRNA expression profiling during human cord blood-derived CD34 cell erythropoiesis. **Exp Hematol**. 2007;35:551-564.

3**0** Zhan M, Miller CP, Papayannopoulou T et al. MicroRNA expression dynamics during murine and human erythroid differentiation. **Exp Hematol**. 2007;35:1015-1025.

3**1** Ketelaar T, Voss C, Dimmock SA et al. Arabidopsis homologues of the autophagy protein Atg8 are a novel family of microtubule binding proteins. **FEBS Lett**. 2004;567:302-306.

3**2** Williams RA, Smith TK, Cull B et al. ATG5 is essential for ATG8-dependent autophagy and mitochondrial homeostasis in Leishmania major. **PLoS Pathog**. 2012;8:e1002695.

3**3** Khoa DB, Takeda M. Expression of autophagy 8 (Atg8) and its role in the midgut and other organs of the greater wax moth, Galleria mellonella, during metamorphic remodelling and under starvation. **Insect Mol Biol**. 2012;21:473-487.

3**4** Kikuma T, Ohneda M, Arioka M et al. Functional analysis of the ATG8 homologue Aoatg8 and role of autophagy in differentiation and germination in Aspergillus oryzae. **Eukaryot Cell**. 2006;5:1328-1336.

3**5** Liu ML, Yao MC. Role of ATG8 and autophagy in programmed nuclear degradation in Tetrahymena thermophila. **Eukaryot Cell**. 2012;11:494-506.

3**6** Behrends C, Sowa ME, Gygi SP et al. Network organization of the human autophagy system. **Nature**. 2010;466:68-76.

3**7** Popovic D, Akutsu M, Novak I et al. Rab GTPase-activating proteins in autophagy: regulation of endocytic and autophagy pathways by direct binding to human ATG8 modifiers. **Mol Cell Biol**. 2012;32:1733-1744.

3**8** Novak I, Kirkin V, McEwan DG et al. Nix is a selective autophagy receptor for mitochondrial clearance. **EMBO Rep**. 2010;11:45-51.

3**9** Hanna RA, Quinsay MN, Orogo AM et al. Microtubule-associated protein 1 light chain 3 (LC3) interacts with Bnip3 protein to selectively remove endoplasmic reticulum and mitochondria via autophagy. **J Biol Chem**. 2012;287:19094-19104.

4**0** Betin VM, Singleton BK, Parsons SF et al. Autophagy facilitates organelle clearance during differentiation of human erythroblasts: Evidence for a role for ATG4 paralogs during autophagosome maturation. **Autophagy**. 2013;9.

4**1** Wang X. miRDB: a microRNA target prediction and functional annotation database with a wiki interface. **RNA**. 2008;14:1012-1017.

4**2** Krek A, Grun D, Poy MN et al. Combinatorial microRNA target predictions. **Nat Genet**. 2005;37:495-500.

4**3** Maragkakis M, Reczko M, Simossis VA et al. DIANA-microT web server: elucidating microRNA functions through target prediction. **Nucleic Acids Res**. 2009;37:W273-276.

4**4** Betel D, Wilson M, Gabow A et al. The microRNA.org resource: targets and expression. **Nucleic Acids Res**. 2008;36:D149-153.

4**5** Kertesz M, Iovino N, Unnerstall U et al. The role of site accessibility in microRNA target recognition. **Nat Genet**. 2007;39:1278-1284.

4**6** Friedman RC, Farh KK, Burge CB et al. Most mammalian mRNAs are conserved targets of microRNAs. **Genome Res**. 2009;19:92-105.

Figure 1. Characteristic of erythroid cells derived from EB9-D0 and EB20-D0. **(A)** Morphology of the erythroid cells generated from hESCs during EB9 and EB20 differentiation. During differentiation into mature cultured RBCs (second step of the protocol), morphological analysis of the cells was performed by May-Grünwald-Giemsa staining. Photographs show representative images (n = 3) of each stage of erythroid maturation on days 4, 8, 15, 18 and 25 (magnification x 630). **(B)** Flow cytometric analysis of EB9- and EB20-derived erythroid cells on day 18. Histograms and percentages of cells expressing erythroid markers (CD71, CD36 and CD235a). Open histograms: negative controls. Solid histograms: positive cells.

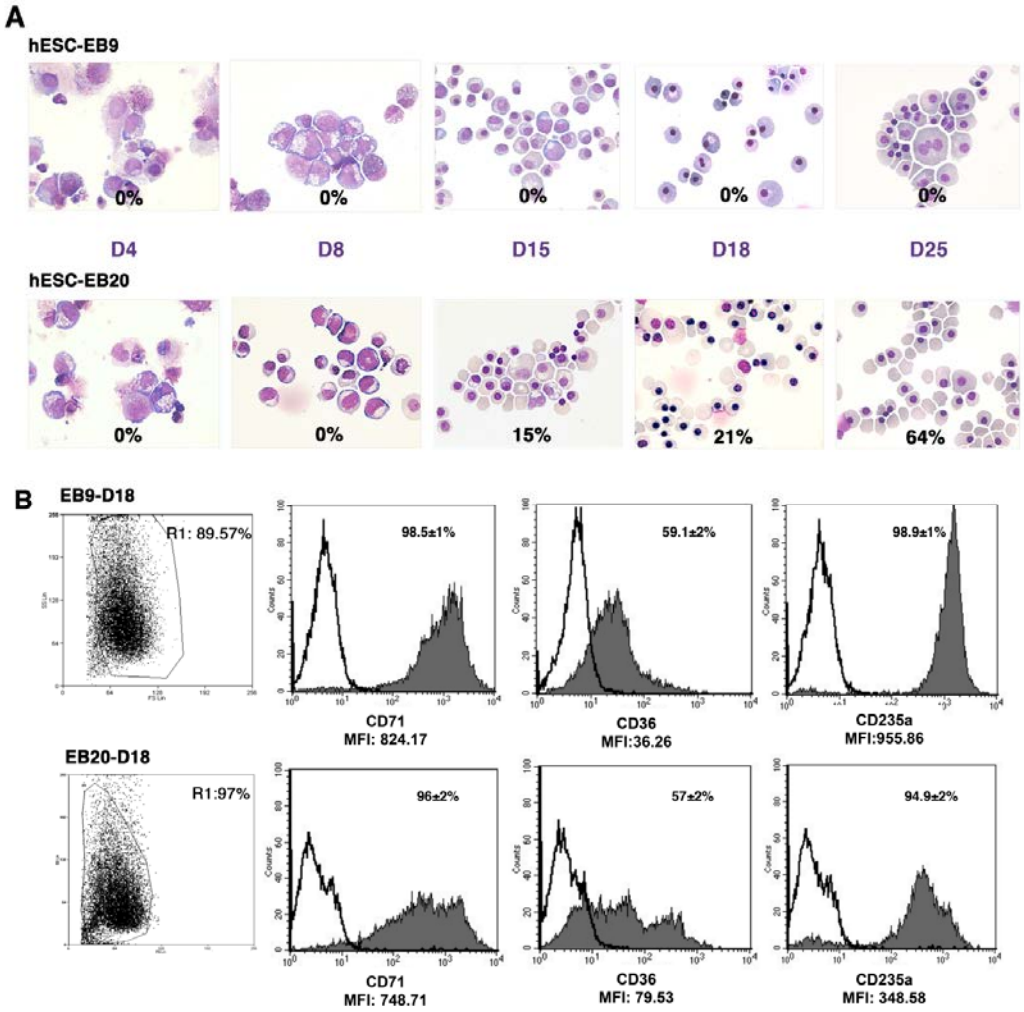

Figure 2. (A) Comparative expression of transcripts as determined by real-time qPCR and microarray analyses. For each gene, the fold change is given between EB20-D18 and EB9-D18 cells. Black bars represent microarray data and dotted bars qPCR; data were determined in triplicate from 3 biological replicates of individual samples. GAPDH was the loading control. The error bar is the standard deviation (SD) (n = 3). **(B)** Venn diagrams illustrating the 1397 overlapping transcripts identified by comparing transcripts up-regulated between EB20-D18 and EB20-D0 cells with transcripts up-regulated between EB20-D18 and EB9-D18 cells. **(C)** Cross-linked gene set enrichment analysis. Enrichment analysis representing the most significant molecular and cellular functions associated with the 1397 overlapping transcripts identified in (B).

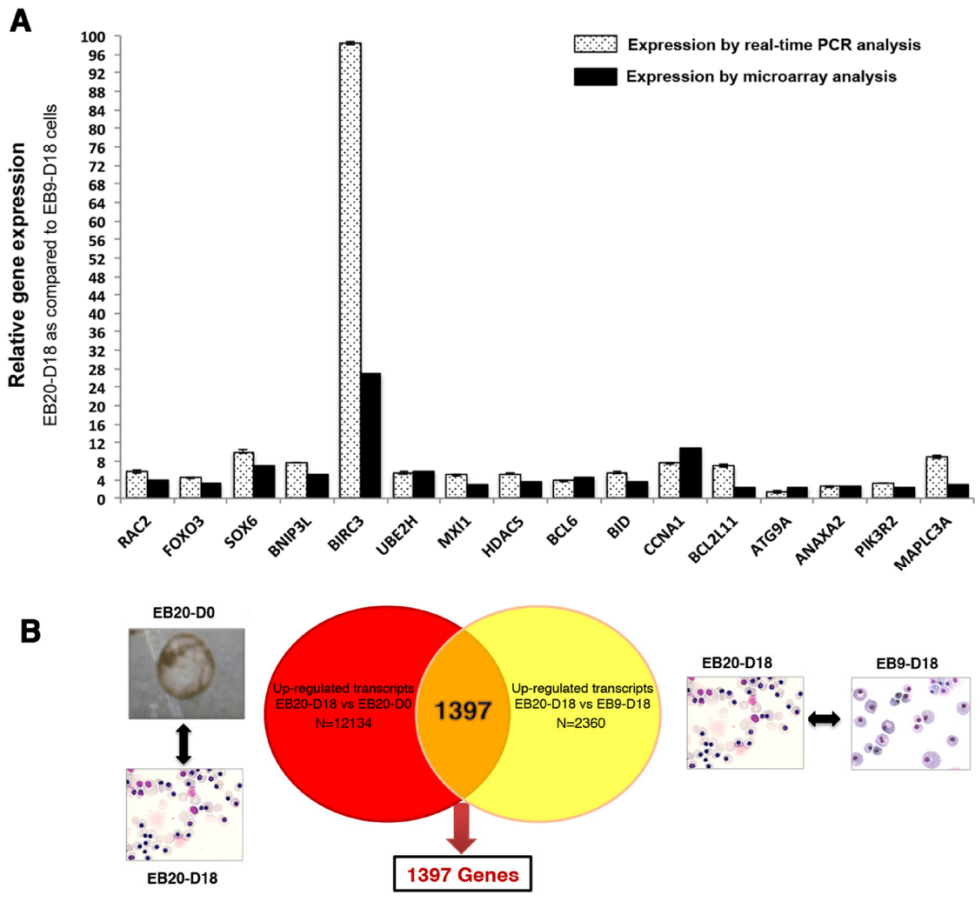

C

GO-Term/Pathway	P-value
Autophagic vacuole	1.58E-05
Autophagy	9.41E-05
FoxO family signaling	1.62E-04
Degradation	7.21E-04
Hemoglobin complex	2.40E-03
E2F transcription factor network	7.35E-03

Figure 3. Functional analysis of miR-30a, miR-34a and miR-9 (A) Morphology of the erythroid cells generated from EB9 cells. May-Grünwald-Giemsa staining of day 25 cultured cells infected with the indicated vectors; representative images are shown (n = 3). **(B)** miR expression as assessed by real-time qPCR in cells transduced with miRZIP-30a, miRZIP-34a, miRZIP-9 and a scramble vector. Relative fold changes in expression (normalized to U6/U48) were calculated by the ^{DD}CT method and values are expressed as 2 ^{DDCT}. The error bar is the standard deviation (SD) (n = 3). (***) $P <$ 0.001 in Student *t*-test (n = 3).

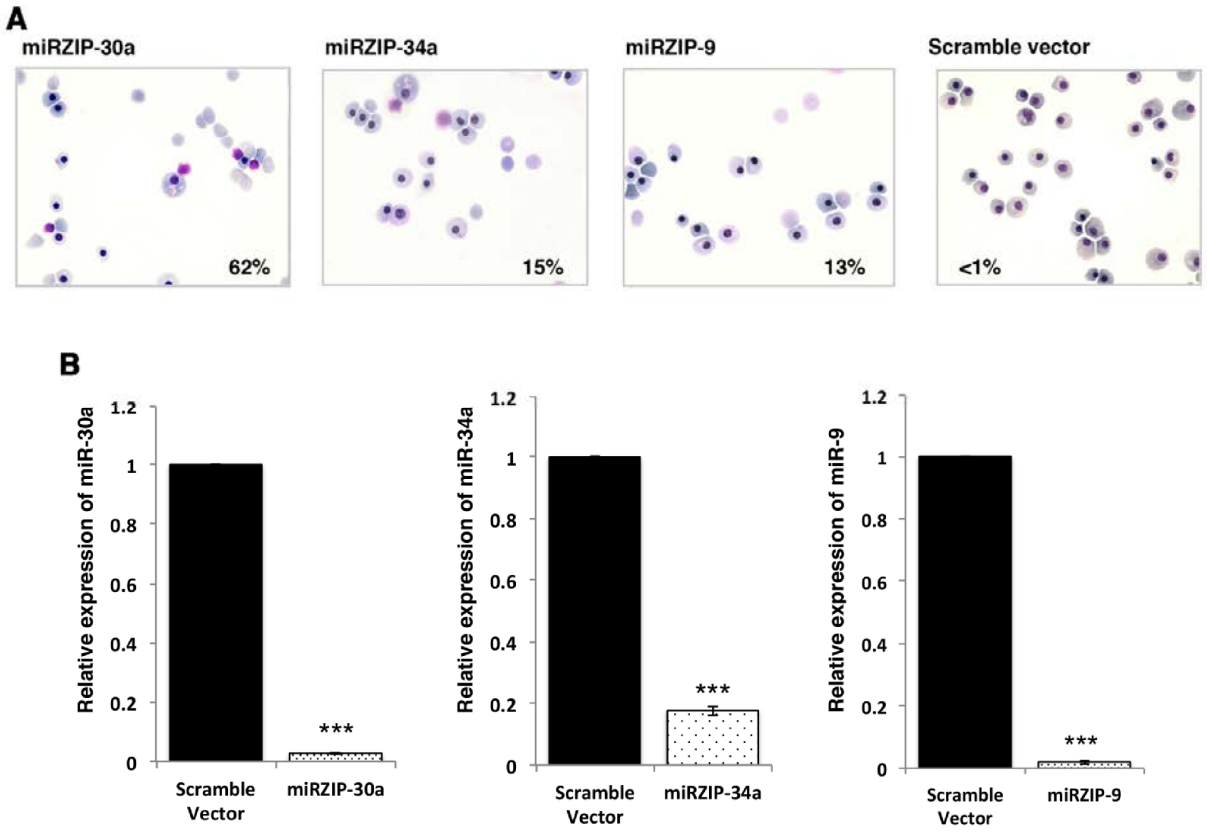

Figure 4. Expression of miRs in erythroid cells. (A) Comparative expression of miR-30a, miR-34a and miR-9 as determined by real-time qPCR in cells derived from H1 and H9 hESCs depending on the duration of EB differentiation (9 days versus 20 days). **(B)** miR-30a expression pattern during erythroid differentiation at different time points (D8-D18) in cells derived from H1 and H9 hESCs as assessed by real-time qPCR; H1-EB20, H1-EB9, H9-EB20 and H9-EB9. **(C)** Kinetics of miR-30a expression during erythroid differentiation of CD34+ cells derived from human cord blood (CB-CD34+) as determined by real-time qPCR and the correlation with enucleation. **(D)** Comparative expression of miR-30a in CB-CD34+, H1-EB9 and H9-EB9 on day 18. U6 was the loading control. The error bar is the SD (n = 3). (***) $P < 0.001$ in Student *t*-test (*n* = 3).

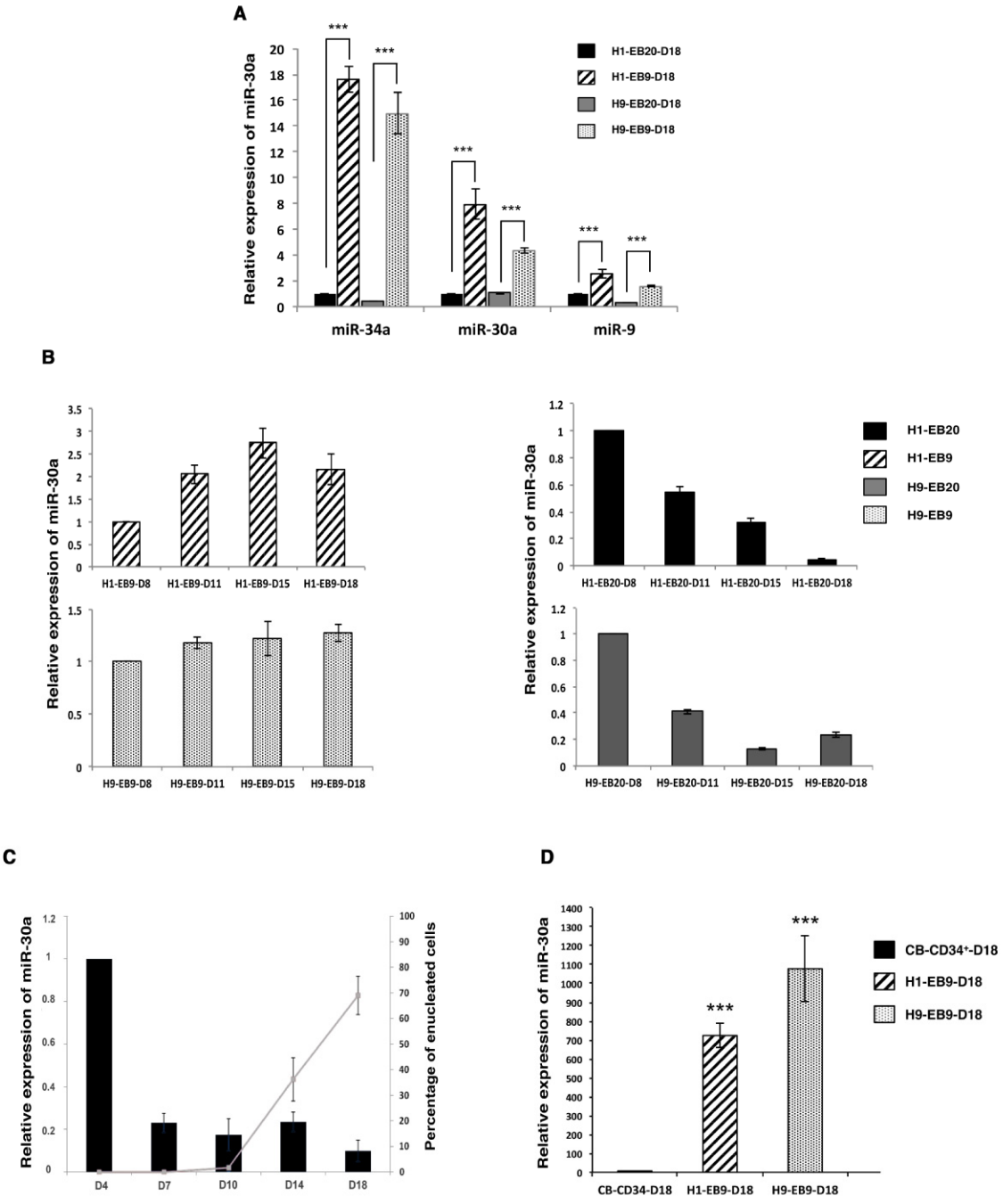

Figure 5. Expression of potential target genes in miRZIP-30a-infected cells. RT–qPCR analysis shows the expression of putative targets of miR-30a on day 25 of *in vitro* culture of erythroid cells infected with the miRZIP-30a virus (hatched bar: miRZIP-30a) as compared to non transduced EB9 control cells (black bar: EB9) and cells infected with a scramble vector (gray bar: Scramble vector). Relative fold changes in expression (normalized to 18s and GAPDH) were calculated by the ^{DD}CT method and values are expressed as 2 ^{DDCT}. The error bar is the SD (n = 3).

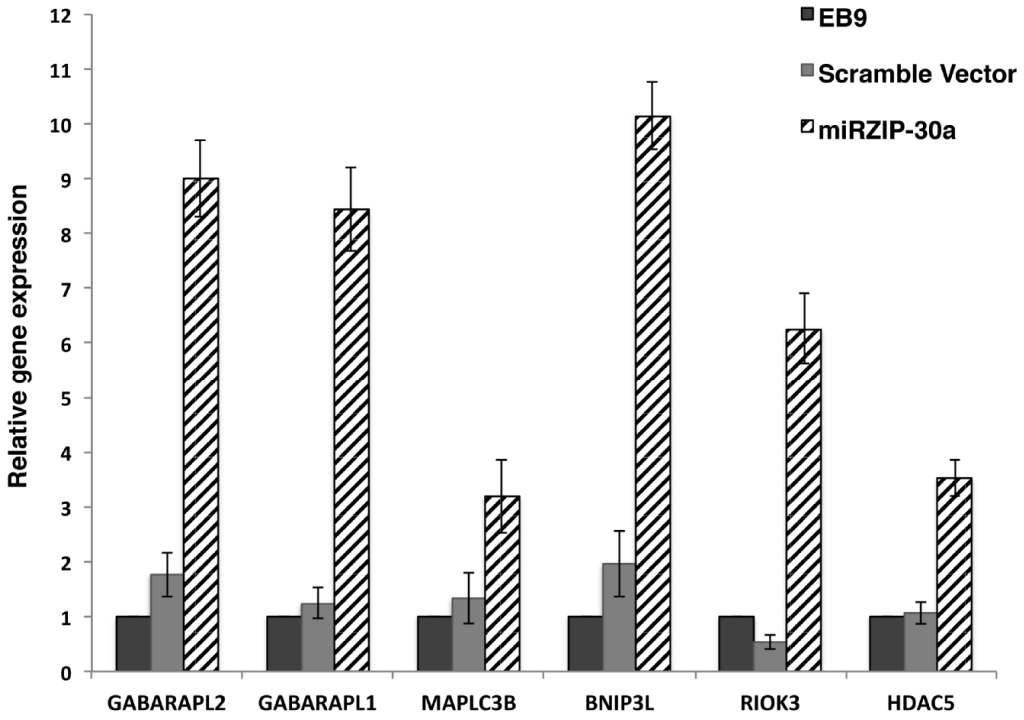

Table 1. Erythroid differentiation of H1 hESCs (A) Flow cytometric analyses of H1 hESCs and cells derived from H1 hESCs Percentages of cells expressing undifferentiated cell markers (SSEA-1, SSEA-4), hematopoietic markers (CD45, CD34) and erythroid markers (CD71, CD36, CD235a) during EB differentiation on day 9 (EB9-D0) and day 20 (EB20-D0), **(B)** Percentage of erythroid cells at different stages of differentiation (pro-erythroblast, basophilic erythroblast, polychromatic erythroblast, orthochromatic erythroblast and reticulocyte) on day15, 18 and 25 in EB20 and EB9 derived cell cultures. **(C)** Total yield of erythroid cells from EB20, EB9, EB9-scramble vector and, EB9-miRZIP30a from D0 to D25 of erythroid differentiation. Lentiviral transfection and GFP+ based cell sorting are performed at D4 and D8 respectively. By day 8 the transfection efficiency for EB9-miRZIP30a and EB9-Scramble vector was 51.2±13 and 55.8±17 respectively.

Results are mean+/- SD of three independent experiments

A

	SSEA-1	SSEA-4	TRA-1-60	TRA-1-81	CD34	CD45	CD34/45	CD71	CD36	CD235a
H1	1.5±1.2	96.2±1	81±2	80±2	0	0.7±0.1	0	73.2±1	0	0
EB9-D0	4.2±0.8	35±4.6	4.4±2.8	5.3±2.9	6.1±0.9	1.9±1	1.5±1	79.7±1.5	0	1.5±1
EB20-D0	14.3±3.5	15.7±2	10.1±2.8	9.7±2	4±0.3	8.1±4	1.7±0.1	64.7±1	4.6±1.2	11.3±1

B

H1-EB20	ProE	BasoE	PolyE	OrthoE	cRBC
D15	4±1	12±4	24±3	48±3	11±3
D18	0	4±3	10±5	66±4	22±3
D25	0	1±2	6±6	40±3	55±11

H1-EB9	ProE	BasoE	PolyE	OrthoE	cRBC
D15	5±1	36±2	40±3	19±3	0
D18	0	12±1	10±4	78±9	0
D25	0	2±1	4±5	93±2	0.6±0.5

C

	Erythroid induction				Erythroid differentiation			
	Total number of cells				Total number of erythroid cells		Enucleation rate (%)	Amplification after transduction (fold)
	D0	D4	D8		D8	D25	D25	D4-D25
H1-EB20	$5x10^7$	$1.1x10^7 \pm 2.8x10^6$	$1.1x10^8 \pm 4.8x10^7$	_	$1x10^7$	$9.0x10^7 \pm 2.9x10^7$	55±11	92.2 ± 20.0
H1-EB9	$5x10^7$	$9.5x10^6 \pm 2.4x10^6$	$8.9x10^7 \pm 3.0x10^7$	-	$1x10^7$	$8.9x10^7 \pm 1.8x10^7$	0.6±0.5	82.1 ± 7.3
H1-E9-Scramble vector	$5x10^7$	$1.0x10^7 \pm 1.3x10^6$	$9.1x10^7 \pm 1.6x10^7$	Cell sorting	$1x10^7$	$8.8x10^7 \pm 2.1x\ 10^7$	0.4±0.3	77.7± 5.7
H1-EB9miRZIP30a	$5x10^7$	$9.2x10^6 \pm 1.5x10^6$	$8.8x10^7 \pm 1.2x10^7$	Cell sorting	$1x10^7$	$7.9x10^7 \pm 1.5x10^7$	51±10	74.6 ± 7.7

Table 2. Enrichment analysis of genes differentially expressed in EB9-D18 as compared to EB20-D18 cells. Enrichment analysis representing the most significant molecular and cellular functions associated with **(A)** transcripts up-regulated between EB9-D18 and EB20-D18 cells and **(B)** transcripts down-regulated between EB9-D18 and EB20-D18 cells.

A

GO-Term	P-value
Regulation of cellular process	2.62E-07
Regulation of biological process	1.23E-06
Regulation of cell development	2.12E-06
Regulation of gene expression	4.78E-06

B

GO-Term	P-value
Immune system process	1.26E-14
Signal transduction	3.75E-14
Immune response	4.42E-11
Response to stimulus	5.35E-10
Cell activation	7.08E-10